





A Handheld Fiber-Optic Probe to Enable Optical Coherence Tomography of Oral Soft Tissue

Julia Walther , Jonas Golde , Marius Albrecht, Bryden C. Quirk, Loretta Scolaro, Rodney W. Kirk, Yuliia Gruda, Christian Schnabel, Florian Tetschke, Korinna Joehrens, Dominik Haim, Michaela Buckova, Jiawen Li , and Robert A. McLaughlin 

Abstract—This study presents a highly miniaturized, handheld probe developed for rapid assessment of soft tissue using optical coherence tomography (OCT). OCT is a

non-invasive optical technology capable of visualizing the sub-surface structural changes that occur in soft tissue disease such as oral lichen planus. However, usage of OCT in the oral cavity has been limited, as the requirements for high-quality optical scanning have often resulted in probes that are heavy, unwieldy and clinically impractical. In this paper, we present a novel probe that combines an all-fiber optical design with a light-weight magnetic scanning mechanism to provide easy access to the oral cavity. The resulting probe is approximately the size of a pen (10 mm × 140 mm) and weighs only 10 grams. To demonstrate the feasibility and high image quality achieved with the probe, imaging was performed on the buccal mucosa and alveolar mucosa during routine clinical assessment of six patients diagnosed with oral lichen planus. Results show the loss of normal tissue structure within the lesion, and contrast this with the clear delineation of tissue layers in adjacent inconspicuous regions. The results also demonstrate the ability of the probe to acquire a three-dimensional data volume by manually sweeping across the surface of the mucosa. The findings of this study show the feasibility of using a small, lightweight probe to identify pathological features in oral soft tissue.

Index Terms—Biomedical optical imaging, medical diagnostic imaging, scanning probe microscopy, fiber optics, optical fiber devices, optical coherence tomography.

I. INTRODUCTION

THE soft tissue of the oral cavity comprises a stratified squamous epithelium overlaying the adjacent connective tissue and submucosa. It is subject to the formation of a wide range of malignant, pre-malignant and benign lesions, which are accompanied by alterations of the subsurface microarchitecture of the tissue. Effective treatment depends on the early detection and reliable differentiation of suspicious lesions from normal mucosa.

Unfortunately, current real-time dental imaging techniques are of limited value in visualizing these lesions. X-ray provides poor soft tissue differentiation and involves exposure to ionizing radiation, while standard ultrasound lacks the spatial resolution to visualize the tissue architecture. In practice, diagnosis is often based on visual assessment under incandescent overhead or halogen illumination, in combination with palpation. However, this provides limited insight into subsurface changes in the tissue and has been shown to have poor diagnostic performance [1]. New technologies that provide early insight into these subsurface

Manuscript received October 8, 2021; revised December 20, 2021; accepted December 21, 2021. Date of publication January 7, 2022; date of current version June 20, 2022. The work of Jonas Golde received a Doctoral Scholarship under Project 100284305, in part by the European Union/European Social Fund (ESF) and the Free State of Saxony. The work of Florian Tetschke was supported by the European Union/European Social Fund (ESF) and the Free State of Saxony within the ESF Junior Research Group “Optical Technologies in Medicine” under Project 100270108. This work was supported in part by the Roland Ernst Foundation Dresden under Project: TOMscan, in part by Australia-Germany Joint Research Cooperation Scheme, in part by the Australian Research Council under Grant CE140100003, and in part by the National Health and Medical Research Council, Australia, under Grants APP1178912, APP2002254, and APP2001646. (Julia Walther and Jonas Golde contributed equally to this work.) (Corresponding author: Julia Walther.)

Julia Walther is with the Department of Medical Physics and Biomedical Engineering, Carl Gustav Carus Faculty of Medicine, Technische Universität Dresden, 01307 Dresden, Germany (e-mail: julia.walther@tu-dresden.de).

Jonas Golde and Florian Tetschke are with the Department of Anesthesiology and Intensive Care Medicine, Clinical Sensing and Monitoring, Carl Gustav Carus Faculty of Medicine, Technische Universität Dresden, Germany.

Marius Albrecht was with the Department of Medical Physics and Biomedical Engineering, Carl Gustav Carus Faculty of Medicine, Technische Universität Dresden, Germany. He is now with the Institute of Pathology, Carl Gustav Carus Faculty of Medicine Technische Universität Dresden, Germany.

Bryden C. Quirk, Loretta Scolaro, and Rodney W. Kirk are with the Australian Research Council Centre of Excellence for Nanoscale BioPhotonics, Faculty of Health and Medical Sciences, and the Institute for Photonics and Advanced Sensing, The University of Adelaide, Australia.

Yuliia Gruda and Christian Schnabel are with the Department of Medical Physics and Biomedical Engineering, Carl Gustav Carus Faculty of Medicine, Technische Universität Dresden, Germany.

Korinna Joehrens is with the Institute of Pathology, Carl Gustav Carus Faculty of Medicine, Technische Universität Dresden, Germany.

Dominik Haim and Michaela Buckova are with the Clinic and Polyclinic of Oral- and Maxillofacial Surgery, Carl Gustav Carus Faculty of Medicine, Technische Universität Dresden, Germany.

Jiawen Li is with the Australian Research Council Centre of Excellence for Nanoscale BioPhotonics, Faculty of Engineering, Computer and Mathematical Sciences, and the Institute for Photonics and Advanced Sensing, The University of Adelaide, Australia.

Robert A. McLaughlin is with the Australian Research Council Centre of Excellence for Nanoscale BioPhotonics, Faculty of Health and Medical Sciences, and the Institute for Photonics and Advanced Sensing, The University of Adelaide, Australia, and also with the School of Engineering, University of Western Australia, Australia.

This article has supplementary downloadable material available at <https://doi.org/10.1109/TBME.2022.3141241>, provided by the authors.

Digital Object Identifier 10.1109/TBME.2022.3141241

changes have the potential to significantly improve diagnostic accuracy [2]. These include optical techniques based on autofluorescence or spectroscopy, although such approaches can suffer low signal-to-noise ratio and are inherently superficial because of limited image penetration depth [3].

Optical coherence tomography (OCT) is a non-invasive subsurface imaging modality [4] commonly used in ophthalmology [5] and cardiology [6] to visualize the structure of focal lesions. It uses reflections of low-power, non-ionizing near infrared (NIR) light to provide real-time 2D and 3D cross-sectional images of subsurface tissue, typically with a spatial resolution of 5-15 microns [3].

There is increasing interest in the potential use of OCT in the oral cavity. Much of this work has focused on characterizing changes or defects in enamel [7], whose optical properties in the visible and NIR range are mainly determined by their mineral content [8]. This includes measuring changes due to remineralization [8], characterizing enamel crack patterns [9] and identifying occlusal caries [10]. OCT also has potential to visualize subgingival calculus as well as root cementum [11] and dental implants when obscured by thin layers of mucosa [12]. Beyond that, a recent review showed a small but growing literature applying OCT to soft tissue pathologies [13], with particular potential to visualize changes in the tissue micro-architecture associated with oral cancer [14]–[18] and immunologically mediated diseases such as oral lichen [19], oral mucosa bullous diseases [20] or Sjögren's syndrome [21].

However, OCT probes published in the dental literature [22]–[25] tend to be impractical, heavy and unwieldy and may require an external mounting to hold them. Often, these systems have been adapted from other applications, such as external scanning of the skin. However, operating within the oral cavity places significant constraints upon any imaging tool [26]. For practical scanning in clinical routine, the probe should preferably be handheld, small and light. Such probes are technically challenging to develop as it places strict limits on the use of bulky, high precision optics and scanning mechanisms [16], [27], [28].

In this study, we have addressed these technical issues to develop a small, light handheld imaging miniprobe developed specifically for oral soft tissue applications. The highly miniaturized focusing optics comprise an all-fiber design with a diameter of 125 μm . The light beam is scanned using a novel magnetic actuation scheme. The entire scanning unit is enclosed in a small metal cylinder, 10 mm \times 140 mm, approximately the size of a pen and weighing only 10 grams. To establish feasibility of the miniprobe, we demonstrate its use through a series of in vivo human measurements, visualizing the differences in tissue microarchitecture between normal and pathological soft tissue of patients with oral lichen planus [29]. To the best of our knowledge, this is the smallest OCT probe developed for use in the oral cavity.

II. MATERIALS AND METHODS

A. System Design

The miniprobe consists of a handheld fiber-optic scanhead interfaced to an OCT scanner console. Miniaturization of the

optics within the scanhead is achieved by splicing very accurate lengths of different types of optical fiber onto the end of a length of single-mode optical fiber (SMF 28, Thorlabs Inc., Newton, NJ, USA) to form a weakly focused light beam. Specifically, the single-mode fiber is terminated with a 350 μm length of no-core fiber (NCF125, Success Prime Corporation, Miaoli County, Taiwan) which enables the light beam to expand, and 150 μm of graded-index (GRIN) fiber (DrakaElite 100/125 μm , Drake Communications Inc., Krum, TX, USA), which subsequently focuses the expanded light beam.

2D OCT imaging is achieved by scanning the fiber laterally using a magnetic scanning system, similar to the system introduced in [30]. A small, rare earth ring magnet (1 mm outer diameter) is affixed around the fiber by adhesive. This is mounted within a 3D printed casing (Form2, Formlabs, Somerville, MA, USA) between three copper wire coils. We have designed the miniprobe with three coils to allow for future development of a spiral scanning pattern to enable 3D scan acquisition. However, in this initial implementation, we connected two of the coils in parallel, effectively reducing this to a 2-coil system appropriate for actuating the fiber in a single plane. A microcontroller (AVR, Microchip Technology Inc., Chandler, AZ, USA) is programmed to drive the coils with a sinusoidal current such that the two channels are 180 degrees out of phase. This alternates the magnetic field and actuates the ring magnet and optical fiber back and forth, enabling 2D OCT scanning. A trigger signal is provided as output from the microcontroller to the acquisition PC at the completion of each sweep. This occurs at a rate of 50 images per second. The fiber probe and scanning mechanism are encased within a stainless-steel cylinder (10 mm \times 140 mm, diameter \times length) whereby imaging is performed through a thin sapphire window (8mm \times 0.15mm (diameter \times width), UQG Optics Ltd., Cambridge, U.K.), which is mounted at a 4° angle to the orientation of the fiber at its central location. This angle was empirically selected to minimize back reflections from the air-window interface. The angle between the light beam and the window will vary slightly as the fiber is deflected, but a 4° angle was found to provide good suppression of the parasitic reflection over the entire range of actuation. A photo and schematic of the probe are shown in Fig. 1.

The miniprobe is interfaced to a Fourier domain OCT system based on a swept-source laser (AXP50125-6, Axsun Technologies Inc., Billerica, MA, USA) with 100 kHz sweep rate, 1285 nm center wavelength and 135 nm sweep range. This is integrated with a custom trigger module using a fiber Bragg grating to generate a phase stable A-scan trigger for the digitizer. The miniprobe is configured to image in common-path mode, using the back-reflection from the fiber-air interface to generate the reference reflection. This removes the need for an additional reference arm to be integrated within the probe, further reducing size and weight. Light from the tissue that has coupled back into the fiber is detected using a balanced photo detector configuration (common-path interferometer module, INT-COM-1300, Thorlabs GmbH, Dachau, Germany) and digitized with a high-speed data acquisition card (ATS9373, Alazar Technologies Inc., Pointe-Claire, QC, Canada) using custom software written in LabVIEW (NI Corp., Austin, TX, USA). The OCT system with

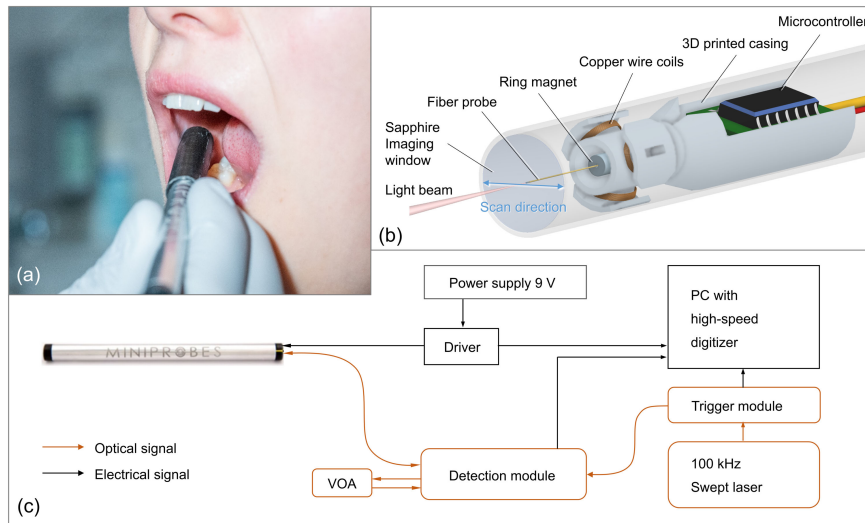


Fig. 1. (a) In vivo application of the handheld miniprobe in the human oral cavity. (b) 3D visualization of internal design of the miniprobe. (c) Schematic of the custom OCT system setup for interferometric imaging with the miniprobe. VOA: variable optical attenuator for balanced detection.

the miniprobe has an axial resolution in air of $11\ \mu\text{m}$ and a lateral resolution of $15\ \mu\text{m}$ (full width half maximum). 2D cross-sectional images were acquired over a 4 mm field of view (FOV) with 1000 depth scans (A-scans) acquired for each image (B-scan). The size of the FOV was quantified by scanning a calibration object with regularly spaced grooves. Note that the scanning configuration is not telecentric, resulting in a fan-shaped scan with an aperture angle of approximately 4.4° . For this reason, only the central 3.3 mm of the scan was used, as distortions within this range were empirically found to be negligible.

B. Subjects

To validate usage of the miniprobe, our study recruited one healthy control and six patients with visually diagnosed oral lichen planus (OLP) for scanning (three male and four female, average age: 65.7, range: 49-81 years). Studies were undertaken at The Clinic and Polyclinic of Oral and Maxillofacial Surgery of the Technische Universität (TU) Dresden. The study was approved by the ethics commission of the Faculty of Medicine of the TU Dresden (EK 96032018 2018-11-16 and EK 39112018 2019-01-22) and informed consent was obtained prior to scanning. OCT images were acquired alongside the buccal mucosa, representing the most common location of OLP in our study, and the alveolar mucosa. In addition, the healthy subject was examined over the buccal and the labial mucosa. None of the volunteers showed oral pigmentation within the investigation areas while all of them were assigned to the fair skin type. Considering typical risk factors for oral soft tissue lesions, three patients occasionally consumed alcohol (Patient I, IV, VI) and one patient smoked approximately five cigarettes per day (Patient II). Five patients described oral symptoms such as periodic pain, oral bleeding and reddened soft tissue within the anamnesis (Patient I, II, III, V, VI). Clinical examination showed different filling materials (amalgam, composite) with

different quality. For treatment of the clinical symptoms of OLP, three patients were being managed with corticosteroids (beclomethasone, triamcinolone) (Patient I, II, VI). Beyond these medications, one patient was receiving amlodipine (Calcium channel blocker) to manage arterial hypertension (Patient V) and one patient had been diagnosed with type 1 diabetes (Patient IV).

C. In Vivo Scanning Protocol

During medical consultation, each subject underwent visual and tactile examination of the oral cavity for suspicious lesions of the oral mucosa. The miniprobe was disinfected (Sekusept Aktiv, Ecolab Deutschland GmbH) and covered with a dental disposable plastic sleeve usually used as surface barrier during bitewing radiography (X-ray Cover, Henry Schein Inc.). OCT imaging was performed both at the center of the lesion and in adjacent, normal-appearing tissue outside of the lesion. The lesion and adjacent tissue were photographed, and visual appearance documented during the examination, and the scanning locations recorded. For Patient I, a biopsy was also acquired at the scanning location within the lesion.

III. RESULTS

Representative images illustrating the ability of the miniprobe to visualize the subsurface structures of normal tissue are presented in Fig. 2. A sequence of images (50 B-scans/second) were acquired as the handheld probe was moved across the inner lower lip (bottom row, Fig. 2(b)–(e)) of the healthy control. The probe was moved by hand in a direction parallel to the fiber actuation, thus providing a sequence of overlapping B-scans. The image sequence was then stitched together to form the extended field-of-view mosaic image in Fig. 2(a), using standard semi-automated image processing techniques [31]. The OCT images show a clear delineation between the epithelial layer (EP), the underlying lamina propria (LP) and the basement

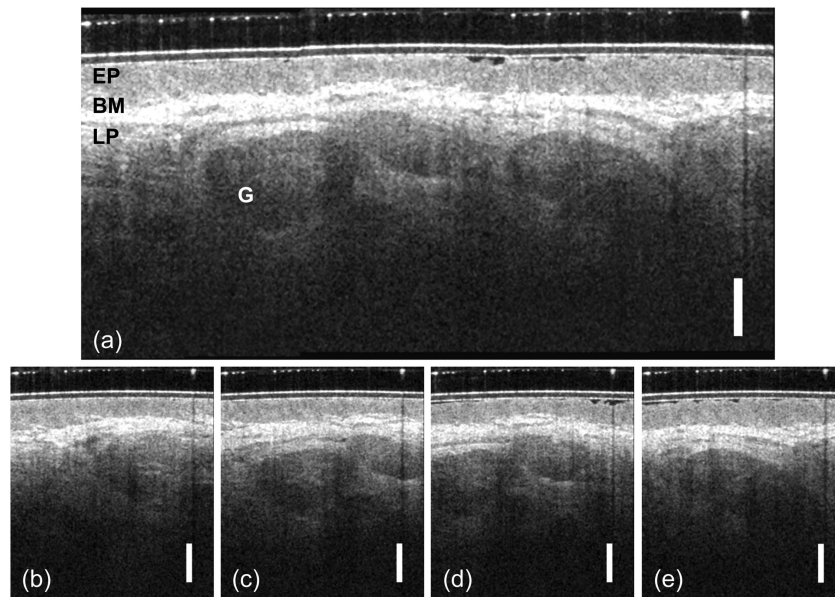


Fig. 2. (a) In vivo OCT cross section of the normal human labial mucosa with an extended lateral field of view (FOV) by means of stitching several overlapping B-scans extracted from a real-time video of OCT scanning (Supplementary file), together. (b)–(e) Single OCT B-scan images used to construct extended field-of-view image. EP: Epithelium, LP: Lamina propria, BM: Basement membrane, G: Glandular structures. Scale bar: 500 μm .

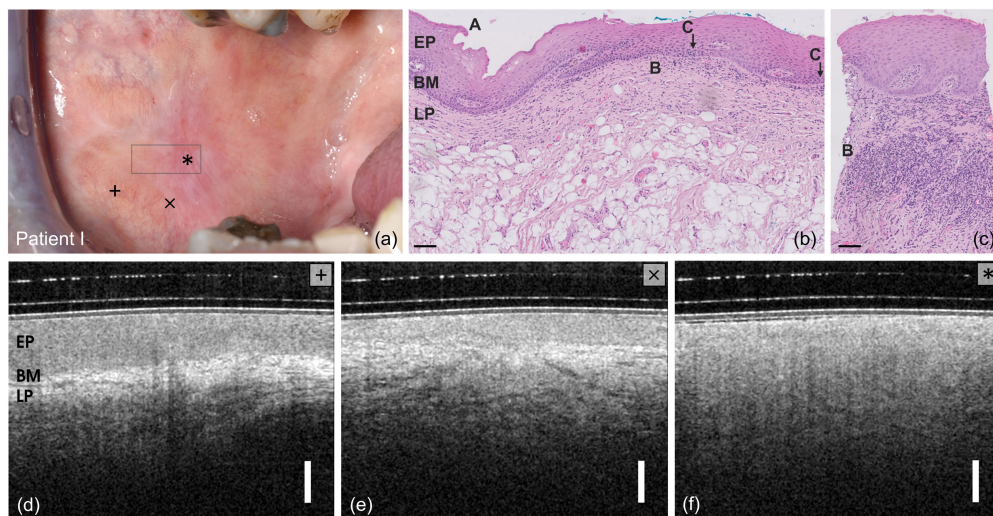


Fig. 3. (a) Photograph of the inner side of the right cheek of Patient I showing the atrophic buccal mucosa. Scanning locations indicated by +, \times , *. * is centered in the OLP. Biopsy location indicated by gray square. (b), (c) H&E histological sections of the biopsy. (d), (e), (f) OCT images of the buccal mucosa from locations +, \times , * respectively. Labels: EP: Epithelium, BM: Basement membrane, LP: Lamina propria. A: Parakeratinized epithelium, B: Subepithelial band of inflammatory lymphocyte infiltrate with C: small overlap on the squamous epithelium. Scale bar: 500 μm .

membrane (BM, interface between EP and LP), as well as glandular structures (G).

Results correlating OCT images, visual appearance and histology from Patient I are shown in Fig. 3. OCT images were acquired in an atrophic appearing buccal lesion consisting of an erythematous area surrounded by keratotic white striations (Wickham's striae), which are typical for the reticular form of OLP. A biopsy of the pathological tissue was acquired immediately after OCT imaging, with histological sections stained using hematoxylin and eosin (H&E). The photo of Fig. 3(a) shows the locations of the biopsy (gray box), OCT imaging of

the lesion (marked as *) and of two adjacent locations showing inconspicuous buccal mucosa (marked as +, \times). Histological sections in Fig. 3(b), (c) from the biopsy sample reveal lichenoid features compatible with initial OLP, such as the parakeratinized epithelium (A), and the existence of a band-like, predominantly lymphocytic chronic inflammatory infiltrate within the subepithelial lamina propria (B) with a slight overlap on the not significantly widened squamous epithelium in combination with occasional basal epithelial cell degeneration (C).

In vivo OCT images of the inconspicuous buccal mucosa (+, \times) show intact layered structures, comprising of a darker,

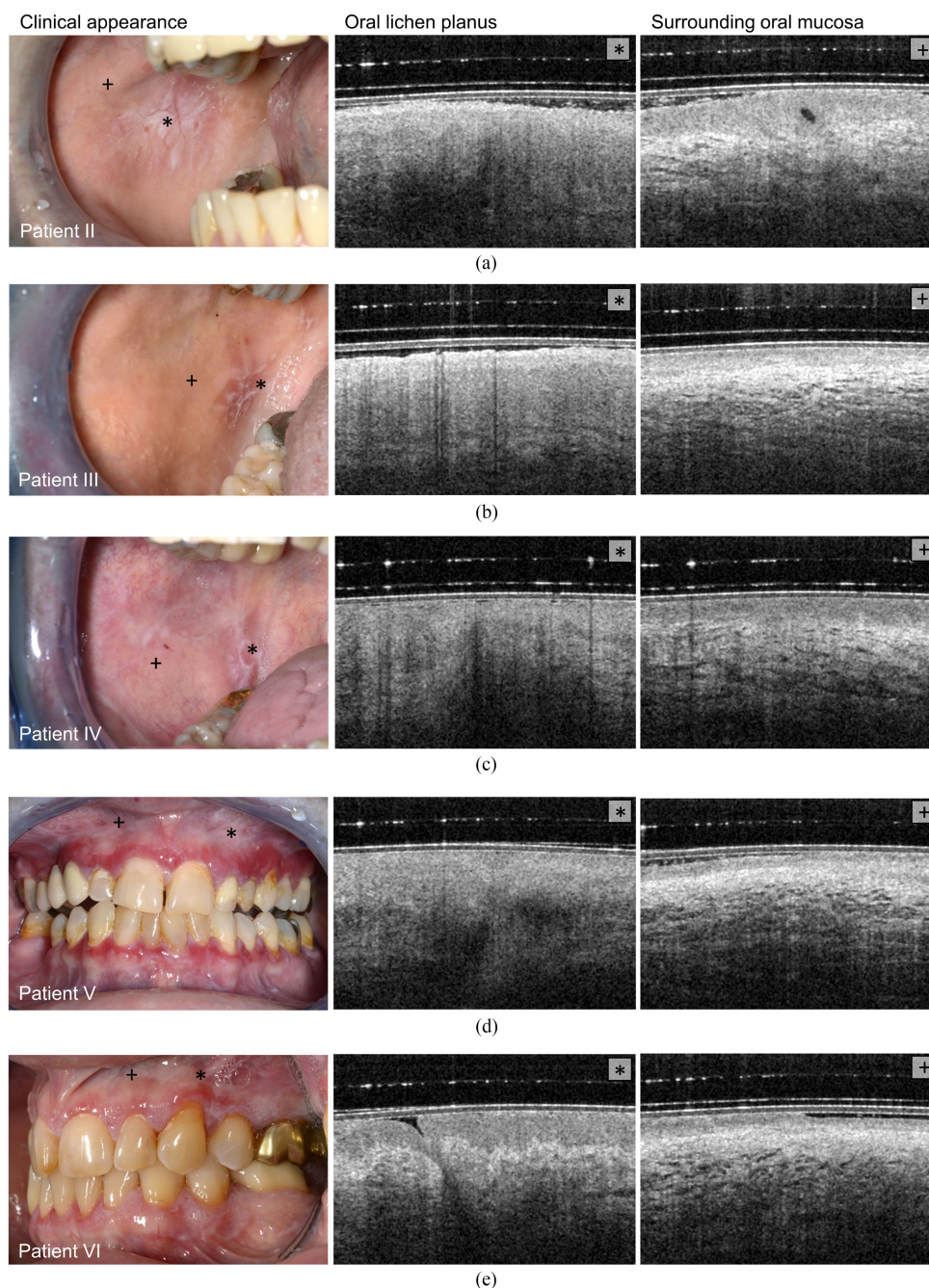


Fig. 4. Photographs and OCT cross sections of five patients clinically diagnosed with symptomatic OLP at the buccal side (a), (b), (c) and the alveolar region (d), (e). Left column: Photographs of the clinical appearance. Middle column: OCT B-scan images of the center of OLP. Right column: OCT B-scans of the clinically inconspicuous oral mucosa surrounding the OLP center.

hyporeflective epithelium (EP), and an underlying brighter hyperreflective lamina propria (LP). Clear delineation of the layers in Fig. 3(d) suggests that the basement membrane is intact. Using the technique described in [32], we quantified the epithelial thickness here to be $395 \mu\text{m}$, using a refractive index of $n = 1.4$ for the epithelium at a wavelength of $\lambda = 1300 \text{ nm}$ [33]. We note that the layers are less distinct in Fig. 3(e). This could be caused by the occasional basal and suprabasal apoptosis of the epithelial cells in combination with an increased capillary proliferation in the subepithelial stroma that is typical for OLP. At the center

of the lesion (Fig. 3(f)), an increased reflectivity is observed in the upper epithelium, which might be caused by keratosis as suggested by [34]. Beyond that, the basement membrane could not be identified, indicating pathological deterioration of the tissue microarchitecture.

Results demonstrating usage of the miniprobe during standard clinical examinations of a further five patients are presented in Fig. 4. OCT images were acquired both in the region of OLP (scan location indicated by *), and in adjacent oral mucosa (scan location indicated by +). Results for each patient are shown on a

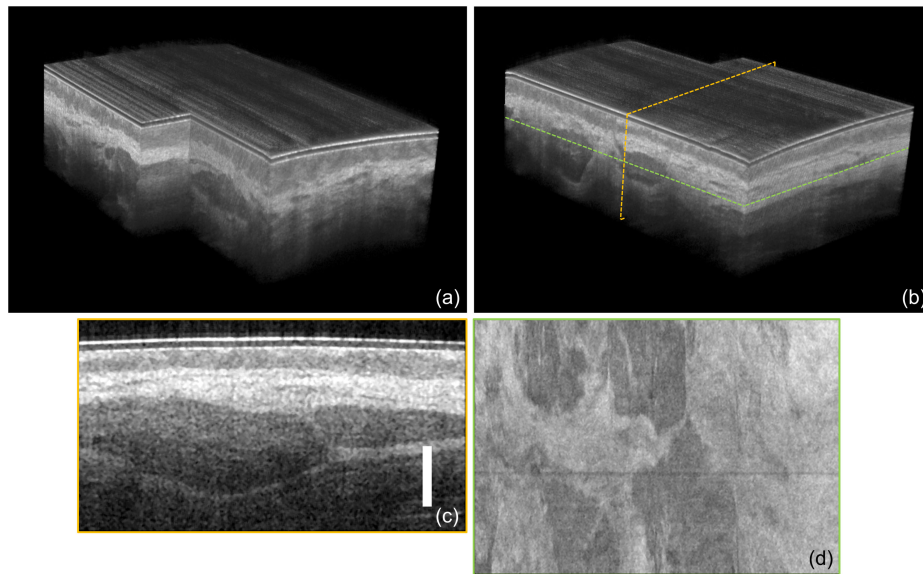


Fig. 5. (a), (b) Volume rendered 3D acquisition of the labial oral mucosa of the healthy volunteer. (c) Cross-sectional view extracted from 3D dataset, corresponding to yellow dashed line in 5b. (d) En face view extracted from 3D dataset, corresponding to green dashed line in 5b, showing characteristic glandular structures within the lamina propria. Scale bar: 500 μm .

separate row, with OCT images of the OLP in the center column, and the adjacent inconspicuous region in the right column. In the adjacent inconspicuous region, OCT images consistently revealed a hyporeflective epithelial layer, indicated by the darker horizontal band of tissue, above the hyperreflective (brighter) lamina propria. The image from Patient II (top row) additionally shows a small, black elliptical structure in the epithelial layer, likely to a fluid-filled salivary gland duct. Comparing the OCT images of the buccal mucosa (Patients II,III,IV) and alveolar mucosa (Patients V and VI), we quantified the mean epithelial thicknesses as 158 μm and 96 μm , respectively. This is in broad agreement with our earlier studies on epithelial thickness using a larger, more unwieldy OCT probe [32].

OCT images of the OLP center region (middle column) showed consistent loss of the healthy tissue microarchitecture to different degrees. Typically, this included degradation of the layered tissue structure, although layers are still partially discernible in Patient VI. We also noted a loss of visibility of the vascular and glandular structures, which appeared in the adjacent region as a texture of dark and bright areas, indicating low optical scattering fluid-filled and high-scattering solid tissue, respectively.

IV. DISCUSSION

In this study, the use of a novel OCT probe, optimized for imaging within the oral cavity, has been explored. Key innovations in the miniprobe have been the integration of a miniaturized, fiber-optic imaging lens with a light-weight, magnetic scanning mechanism to enable a small, pen-sized scanhead that weighs only 10 g. This is in contrast with previous OCT probes that typically consist of a short, compact main body containing larger optical components and scanning mechanisms, coupled to a long, thin imaging tube to provide access to the oral cavity [25], [27], [28], [35]. The potential impact of the significant reductions

we have achieved in weight and size of an OCT probe may help transition OCT from a research tool to an imaging modality that can be easily integrated into clinical practice.

An advantage of such a maneuverable probe is the ability to acquire freehand 3D scans of the tissue microarchitecture by manually moving the probe across the mucosa. An example of a 3D scan acquired with the miniprobe is shown in Fig. 5, constructed by rapidly acquiring a sequence of 2D B-scans images (50 B-scans/second) as the probe was slid across the labial oral mucosa. During this acquisition, the probe was moved by hand, orthogonally to the direction of fiber actuation, providing a contiguous sequence of parallel B-scans. Volume rendered images from two opposing viewpoints are presented in Fig. 5(a), (b). A cross-sectional 2D image is extracted in Fig. 2(c), with the location of the cross-section shown by the orange dashed line in Fig. 5(a). An en face view extracted from the 3D acquisition is presented in Fig. 5(d). This en face image shows the tissue structure at a specific depth over the entire field of view, indicated by the green dashed line in Fig. 5(b), and allows visualization of the glandular structures within the lamina propria. The acquisition of freehand 3D volumes with the miniprobe enables arbitrarily long 3D acquisitions, limited only by how far the probe can be moved. Because the probe is in light contact with the tissue, we found it easy to sweep across the tissue and did not identify any vertical discontinuities in the structures visible in the image that would have indicated uncontrolled axial movement.

Within our feasibility trial, we were able to clearly delineate the layered structures of the epithelium and the lamina propria in the oral mucosa adjacent to OLP and identify embedded anatomical structures such as minor salivary glands. In regions identified as OLP, we observed pathological deterioration of the subsurface microarchitecture, evidenced most clearly as reduced demarcation between layers and a loss of vascular and glandular

structures. This correlates with the results of previous studies using larger OCT probes that have been adapted from other clinical applications [19], [25].

V. CONCLUSION

We have presented a novel OCT probe designed for use in the oral cavity, integrating a highly miniaturized fiber-optic lens design with a lightweight scanning mechanism. The miniprobe achieves a form-factor well suited for dental applications, and we found its small size appropriate even for access to narrow sites such as regions next to the dental arch. Feasibility of the probe was validated in a study of patients diagnosed with oral lichen planus. Our results showed that OCT was able to visualize the loss of delineation between the epithelium and lamina propria and changes in the presence of glandular structures, and contrast these against the intact layered tissue structures in adjacent regions of tissue. The thickness of the epithelium was also quantified with OCT and found to vary between anatomical regions. Other work has shown correlation between OCT and histopathology in oral premalignancy and malignancy [36], suggesting that a lightweight tool such as the miniprobe has great potential to aid in guiding biopsies in standard clinical practice.

CONFLICT OF INTEREST

J. Walther, J. Golde, M. Albrecht, L. Sclaro, Y. Gruda, C. Schnabel, F. Tetschke, K. Joehrens, D. Haim, M. Buckova and J. Li declare that they have no conflict of interest. B. C. Quirk, R. W. Kirk and R. A. McLaughlin are cofounders of the company, Miniprobes Pty Ltd. Miniprobes Pty Ltd did not contribute funding to this study.

REFERENCES

- [1] J. B. Epstein *et al.*, "The limitations of the clinical oral examination in detecting dysplastic oral lesions and oral squamous cell carcinoma," *J. Amer. Dent. Assoc.*, vol. 143, no. 12, pp. 1332–1342, 2012.
- [2] N. Bhatia *et al.*, "Advances in optical adjunctive AIDS for visualisation and detection of oral malignant and potentially malignant lesions," *Int. J. Dent.*, vol. 2013, 2013, Art. no. 194029.
- [3] P. Wilder-Smith *et al.*, "Optical diagnostics in the oral cavity: An overview," *Oral. Dis.*, vol. 16, no. 8, pp. 717–728, 2010.
- [4] W. Drexler and J. G. Fujimoto, *Optical Coherence Tomography: Technology and Applications*. Amsterdam, Switzerland: Springer International Publishing, 2015.
- [5] N. C. Y. Chan and C. K. M. Chan, "The use of optical coherence tomography in neuro-ophthalmology," *Curr. Opin. Ophthalmol.*, vol. 28, no. 6, pp. 552–557, 2017.
- [6] L. Vignali *et al.*, "Research and clinical applications of optical coherence tomography in invasive cardiology: A review," *Curr. Cardiol. Rev.*, vol. 10, no. 4, pp. 369–376, 2014.
- [7] M. Machoy *et al.*, "The use of optical coherence tomography in dental diagnostics: A state-of-the-art review," *J. Healthcare Eng.*, vol. 2017, 2017, Art. no. 7560645.
- [8] R. S. Jones and D. Fried, "Remineralization of enamel caries can decrease optical reflectivity," *J. Dent. Res.*, vol. 85, no. 9, pp. 804–808, 2006.
- [9] M. S. Segarra *et al.*, "Three-dimensional analysis of enamel crack behavior using optical coherence tomography," *J. Dent. Res.*, vol. 96, no. 3, pp. 308–314, 2017.
- [10] M. N. Luong *et al.*, "Diagnosis of occlusal caries with dynamic slicing of 3d optical coherence tomography images," *Sensors*, vol. 20, no. 6, 2020, Art. no. 1659.
- [11] M. Tsubokawa *et al.*, "In vitro and clinical evaluation of optical coherence tomography for the detection of subgingival calculus and root cementum," *J. Oral. Sci.*, vol. 60, no. 3, pp. 418–427, 2018.
- [12] M. Sanda *et al.*, "The effectiveness of optical coherence tomography for evaluating peri-implant tissue: A pilot study," *Imag. Sci. Dent.*, vol. 46, no. 3, pp. 173–178, 2016.
- [13] E. Gentile *et al.*, "The potential role of in vivo optical coherence tomography for evaluating oral soft tissue: A systematic review," *J. Oral. Pathol. Med.*, vol. 46, no. 10, pp. 864–876, 2017.
- [14] A. E. Heidari *et al.*, "Optical coherence tomography as an oral cancer screening adjunct in a low resource settings," *IEEE J. Sel. Top. Quantum Electron.*, vol. 25, no. 1, Jan./Feb. 2019, Art. no. 7202008.
- [15] C. K. Lee *et al.*, "Diagnosis of oral precancer with optical coherence tomography," *Biomed. Opt. Exp.*, vol. 3, no. 7, pp. 1632–1646, 2012.
- [16] J. M. Ridgway *et al.*, "In vivo optical coherence tomography of the human oral cavity and oropharynx," *Arch. Otolaryngol. Head. Neck. Surg.*, vol. 132, no. 10, pp. 1074–1081, 2006.
- [17] M. T. Tsai *et al.*, "Differentiating oral lesions in different carcinogenesis stages with optical coherence tomography," *J. Biomed. Opt.*, vol. 14, no. 4, 2009, Art. no. 044028.
- [18] V. Volgger *et al.*, "Evaluation of optical coherence tomography to discriminate lesions of the upper aerodigestive tract," *Head Neck*, vol. 35, no. 11, pp. 1558–1566, 2013.
- [19] A. Gambino *et al.*, "In-vivo usefulness of optical coherence tomography in atrophic-erosive oral lichen planus: Comparison between histopathological and ultrastructural findings," *J. Photochem. Photobiol. B.*, vol. 211, 2020, Art. no. 112009.
- [20] D. Di Stasio *et al.*, "Optical coherence tomography imaging of oral bullous diseases: A preliminary study," *Dentomaxillofacial Radiol.*, vol. 49, no. 2, 2020, Art. no. 20190071.
- [21] I. Grulkowski *et al.*, "Quantitative assessment of oral mucosa and labial minor salivary glands in patients with Sjogren's syndrome using swept source OCT," *Biomed. Opt. Exp.*, vol. 5, no. 1, pp. 259–274, 2013.
- [22] K. Li *et al.*, "Low-cost, ultracompact handheld optical coherence tomography probe for in vivo oral maxillofacial tissue imaging," *J. Biomed. Opt.*, vol. 25, no. 4, 2020, Art. no. 046003.
- [23] Y. Nakajima *et al.*, "Detection of occlusal caries in primary teeth using swept source optical coherence tomography," *J. Biomed. Opt.*, vol. 19, no. 1, 2014, Art. no. 16020.
- [24] H. Schneider *et al.*, "An intraoral OCT probe to enhanced detection of approximal carious lesions and assessment of restorations," *J. Clin. Med.*, vol. 9, no. 10, 2020, Art. no. 3257.
- [25] J. Walther *et al.*, "In vivo imaging in the oral cavity by endoscopic optical coherence tomography," *J. Biomed. Opt.*, vol. 23, no. 7, pp. 1–13, 2018.
- [26] D. Demian *et al.*, "Design and testing of prototype handheld scanning probes for optical coherence tomography," in *Proc. Inst. Mech. Eng. H.*, 2014, pp. 743–753.
- [27] D. Wang *et al.*, "Endoscopic swept-source optical coherence tomography based on a two-axis microelectromechanical system mirror," *J. Biomed. Opt.*, vol. 18, no. 8, 2013, Art. no. 86005.
- [28] M. T. Tsai *et al.*, "Noninvasive structural and microvascular anatomy of oral mucosae using handheld optical coherence tomography," *Biomed. Opt. Exp.*, vol. 8, no. 11, pp. 5001–5012, 2017.
- [29] S. Muller, "Oral lichenoid lesions: Distinguishing the benign from the deadly," *Mod. Pathol.*, vol. 30, no. s1, pp. S54–S67, 2017.
- [30] A. Acemoglu *et al.*, "Towards a magnetically-actuated laser scanner for endoscopic microsurgery," *J. Med. Robot. Res.*, vol. 3, no. 2, 2018, Art. no. 1840004.
- [31] P. Thevenaz and M. Unser, "User-friendly semiautomated assembly of accurate image mosaics in microscopy," *Microsc. Res. Tech.*, vol. 70, no. 2, pp. 135–146, 2007.
- [32] M. Albrecht *et al.*, "In vivo endoscopic optical coherence tomography of the healthy human oral mucosa: Qualitative and quantitative image analysis," *Diagnostics*, vol. 10, no. 10, 2020, Art. no. 827.
- [33] S. Prestin *et al.*, "Measurement of epithelial thickness within the oral cavity using optical coherence tomography," *Head Neck*, vol. 34, no. 12, pp. 1777–1781, 2012.
- [34] Z. Hamdoon *et al.*, "Structural validation of oral mucosal tissue using optical coherence tomography," *Head. Neck. Oncol.*, vol. 4, 2012, Art. no. 29.
- [35] L. M. Higgins and M. C. Pierce, "Design and characterization of a handheld multimodal imaging device for the assessment of oral epithelial lesions," *J. Biomed. Opt.*, vol. 19, no. 8, 2014, Art. no. 086004.
- [36] P. Wilder-Smith *et al.*, "In vivo diagnosis of oral dysplasia and malignancy using optical coherence tomography: Preliminary studies in 50 patients," *Lasers Surg. Med.*, vol. 41, no. 5, pp. 353–357, 2009.